ORNL/TM-2023/3113

Progress on Producing an ODS Ferritic Alloy by High Deformation Processing of Reactive Powders

David Hoelzer
Caleb Massey
Thak Sun Byun
Holden Hyer

September 2023

M4FT-23OR060101042

OAK RIDGE National Laboratory

ORNL IS MANAGED BY UT-BATTELLE LLC FOR THE US DEPARTMENT OF ENERGY

ORNL/TM-2023/3113

Materials Science and Technology Division
Innovative Nuclear Materials Program

PROGRESS ON PRODUCING AN ODS FERRTIC ALLOY BY HIGH DEFORMATION PROCESSING OF REACTIVE POWDERS

David Hoelzer
Caleb Massey
Thak Sun Byun
Holden Hyer

September 2023

M4FT-23OR060101042

Prepared by
OAK RIDGE NATIONAL LABORATORY
Oak Ridge, TN 37831
managed by
UT-BATTELLE LLC
for the
US DEPARTMENT OF ENERGY
under contract DE-AC05-00OR22725

CONTENTS

LIST OF FIGURES

ACKNOWLEDGMENTS

This research was sponsored by the US Department of Energy Office of Nuclear Energy's Innovative Nuclear Materials Program under contract DE-AC05-00OR22725 with UT-Battelle LLC. The authors thank Jovid Rakhmonov and Yukinori Yamamoto for their thoughtful reviews of this report before publication and Holden Hyer for 3D printing of the 316L stainless-steel cans.

ABSTRACT

Oxide dispersion-strengthened (ODS) ferritic alloys, such as 14YWT, are considered as benchmarks for fuel cladding and core structural materials in advanced nuclear energy reactor systems that require high-temperature strength and creep properties as well as resistance to radiation damage. Unfortunately, the popular processing method of mechanical alloying (MA) is time-consuming, incurs high manufacturing costs, and typically produces anisotropy in the microstructure and mechanical properties of ODS ferritic alloys. These considerations hinder their acceptance in many high-performance, high-temperature materials for advanced nuclear energy reactors. This work package is pursuing an alternative solid-state processing to MA involving high deformation at high temperatures for producing an ODS ferritic alloy for fuel cladding. This report summarizes the concept for this processing method and the progress toward selecting the reactive and ferritic alloy powders, preparing 316L stainless steel cans for filling with blended powder followed by degassing, and choosing the heat treatments and forging parameters for performing the first two forging experiments. The preliminary results of optical microscopy performed on polished samples that were cut in three orthogonal directions revealed remnant porosity in both samples. The analysis of the porosity using ImageJ revealed a lesser amount of ~2.49% in the HiLoMe-1 sample that was processed with the three heat treatments and forging parameters compared to ~5.70% for the Hi-1 sample that was processed with only the first sintering heat treatment and forging parameter. These initial results will provide insights that can be leveraged to improve the densification of the powders in future forging experiments that will be continued into FY24 for determining the optimum heat treatments and forging parameters coupled with detailed microstructure characterization studies for producing the ODS ferritic alloy.

1. INTRODUCTION

Advanced oxide dispersion-strengthened (ODS) ferritic alloys, such as 14YWT, are being developed for cladding and core structural materials in several nuclear energy reactor systems because of their improved high-temperature strength and creep properties, as well as their resistance to radiation damage [1-11]. The advanced ODS 14YWT ferritic alloy was developed at Oak Ridge National Laboratory (ORNL) starting in the early 2000s [6,8]. The most popular processing method for producing ODS ferritic alloys, such as 14YWT, is by mechanical alloying (MA), mainly due to the very low solubility limit of oxygen in body-centered cubic (BCC) ferritic alloys that prevents this class of alloys from being produced by conventional casting and fabrication processes. The 14YWT ferritic alloy consists of a microstructure that contains a high concentration of nano-size Ti-Y oxide particles and ultra-fine grains. These qualities result in high-temperature strength and creep properties as well as high interfacial area associated with these nano-structural features, providing the high point defect sink strength that is beneficial to radiation tolerance (Figure 1). This approach is a solid-state processing method that involves high-kinetic energy ball milling of alloyed powders with a small quantity of oxide, that is, yttria (Y_2O_3), powder for typically long durations followed by consolidation - for example by extrusion or hot isostatic pressing (HIP) to produce solid products. Consequently, the time-consuming processing procedure and the associated high manufacturing costs of the MA approach hinder ODS alloys' acceptance in many high-performance, high-temperature materials technologies, especially advanced nuclear energy reactors, despite the enormous benefits these alloys offer in terms of high-temperature strength, creep properties, and microstructural stability.

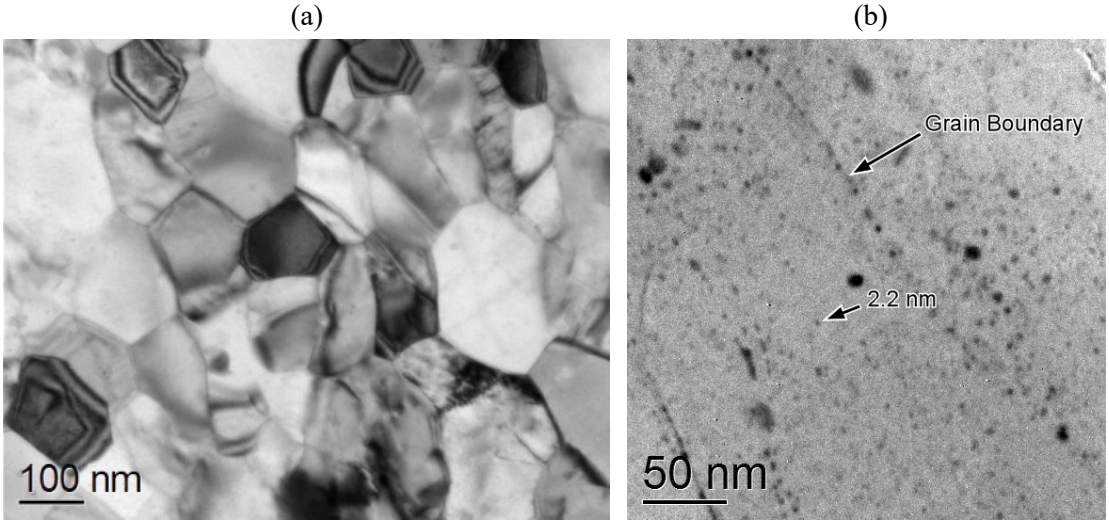

Figure 1. The microstructure characteristics of 14YWT. (a) Transmission electron microscopy (TEM) bright-field image of ultra-small grains and (b) energy-filtered TEM Fe-M jump ratio map of the nanoclusters within the grains and on grain boundaries.

Several recent R&D approaches have attempted to overcome the time-consuming process and high manufacturing cost of the MA approach for producing ODS ferritic alloys. The fundamental concepts with many of these R&D studies involve melting and subsequent solidification processes and modern additive manufacturing (AM) approaches [12–18]. However, the main problem encountered with these alternative processing methods is melting either constituent elements of an ODS alloy or powders that have been MA, which favors lack of control over the size and distribution of the oxide particles in the ferritic alloy after solidification. Although modern AM methods may produce near-nano-size oxide particle dispersions, their size and spatial distributions are heterogeneous in the solidified microstructure, thereby leading to mechanical properties that often lack good strength and ductility properties.

This work package investigates an alternative solid-state processing method based on high deformation at high temperatures to support producing an ODS ferritic alloy for fabrication of fuel cladding. The concept for this alternative processing method consists of (a) high-compaction forging to induce large deformation strains at high strain rates; (b) one or more reactive powders mixed with a ferritic alloy powder that can dissociate during high deformations at elevated temperatures; and (c) investigation of a new solid state processing idea involving migrating grain boundaries during dynamic recrystallization processes that cause the dissolution of the reactive powder and subsequent transport of the constituent solutes through the microstructure. If this idea is successful, then a final heat treatment will nucleate the dispersion of nano-size oxide particles in the ferritic alloy microstructure. Furthermore, the use of forging will enable scale-up production of ODS alloys with a variety of compositions including FeCrAl and alumina-forming austenitic (AFA) stainless steels.

In this report, the initial progress toward developing the solid-state, hot-deformation compaction by forging of gas-atomized ferritic alloy powder blended with a reactive powder for producing an ODS ferritic alloy is summarized.

2. HIGH DEFORMATION PROCESSING OF REACTIVE POWDERS APPROACH

There are two concepts in materials science that this work package is based on: (1) reactive powders induced by ball milling and (2) migrating grain boundaries induced by dynamic recrystallization.

A study involving high-kinetic energy ball milling for reactive milling of intermetallic and oxide powders was investigated as a method to form a Ni-based ODS alloy [19]. It was found in that study that the severe deformations caused by impacts of a large tungsten carbide (WC) ball and powders of Ni_2Y intermetallic and NiO powders led to solid-state mechanisms that caused the chemical exchanges between Ni and Y from the intermetallic powder and Ni and O from the oxide powder. To achieve this reaction, the Ni_2Y and NiO powders were ball-milled for 144 h in vacuum at 30°C and 100°C with a calculated milling intensity of 1880 m/s^2 [19]. The concept of the study was to induce solute transport between the constituent solutes of the dissolved Ni_2Y and NiO powders that would result in a dispersion of Y_2O_3 oxides in the Ni matrix. However, the results obtained by energy-filtered transmission electron microscopy (EFTEM) showed that the opposite occurred: that is, ~10 nm Ni grains surrounded by a nearly continuous amorphous Y-O layer with a similar length-scale. Figure 2 shows a composite RGB map of the Ni L jump ratio (Red), the Y L jump ratio (Green) and the O K jump ratio (Blue) element maps obtained by EFTEM that shows the final microstructure of the Ni grains surrounded the Y-O layers, which possesses a turquoise color from the overlay of green and blue maps. These results demonstrate that severe deformations can fracture and subsequently dissolve reactive powders followed by solid-state short-range diffusion of constituent elements in the microstructure.

In another study, factors that lead to abnormal grain growth during processing of ODS alloys showed that mobile grain boundaries due to application of stresses can produce intragranular precipitation [20]. The study demonstrated the important role of migrating grain boundaries on dissolution and re-precipitation of oxide particles during thermal mechanical treatments (TMT). For this mechanism to work, the solubility of the over-sized Y atoms in the matrix increased on the grain boundary so that as the migrating grain boundary moved via a driving force, the concentration of Y increased to the higher solubility limit. Upon reaching a balance between grain boundary migration and Zener pinning, the dissolved Y will nucleate and/or lead to coarsening of surrounding Y-Ti oxide particles. The driving force for migrating grain boundaries may be static recrystallization during Ostwald ripening of the grains as well as dynamic recrystallization, which involves both stresses and temperatures.

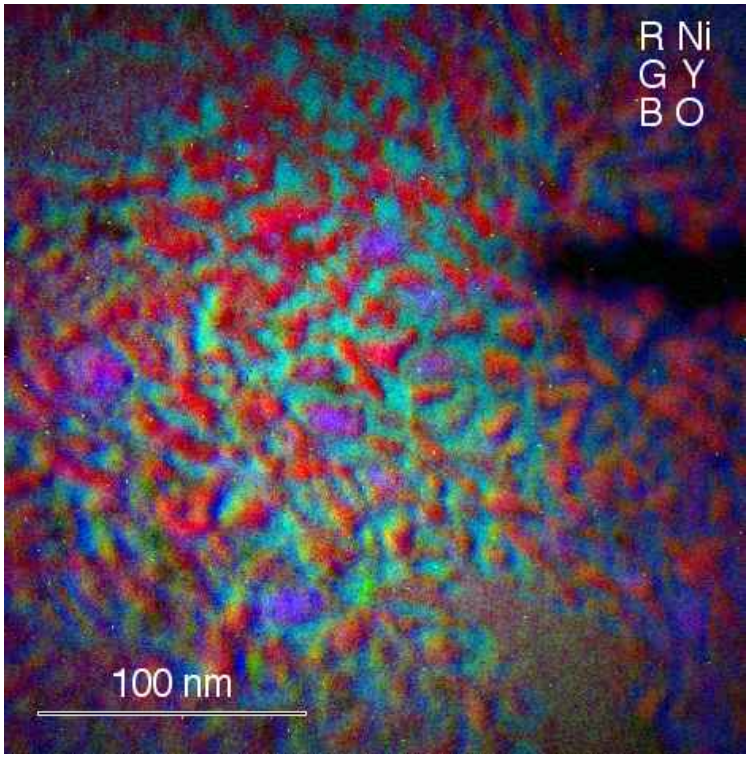

Figure 2. Composite EFTEM map with RGB colorization using the Ni L jump ratio (Red), Y L jump ratio (Green) and O K jump ratio (Blue) element maps after reactive milling of the Ni_2Y intermetallic and NiO powders.

Although static recrystallization may lead to coarsening of precipitates, our research plan is to investigate dynamic recrystallization as a means of transporting solutes around the microstructure, away from conventional grain boundaries. Therefore, the proposed research aims to develop a solid-state processing route for producing nano-size oxide dispersions and nanograin structures in a ferritic alloy by severe hot-deformation compaction of gas-atomized alloyed powder blended with two reactive powders. The processing route will employ variable temperatures during compaction of the powders, concurrent with microstructural characterization studies that provide feedback for optimization of the nano-size oxide dispersion.

3. PROCEDURES

The powders used in the initial forging experiments consisted of a ferritic alloy with nominal composition Fe-10Cr-1W-0.3Ti-0.2V (wt. %) and yttrium iron garnet (YIG) $Y_3Fe_5O_{12}$. The ferritic alloy powder was gas-atomized by ATI Powder Metals, whereas the YIG powder was purchased from American Elements. The YIG phase has a BCC crystal structure with $Ia\bar{3}d$ space group. Figure 3 shows the unit cell of the YIG phase. It has a lattice parameter of ~1.237 nm that contains 160 atoms distributed on three sublattices. The space group symmetry indicates a-glide planes on the four-fold axes and d-glide planes on the two-fold axes. Together, these characteristics of the YIG phase are responsible for the low fracture toughness of ~0.74 $MPa \bullet m^{1/2}$, which indicates that the unit cell can fracture easily, leading to dissolution in the lattice of the ferritic alloy.

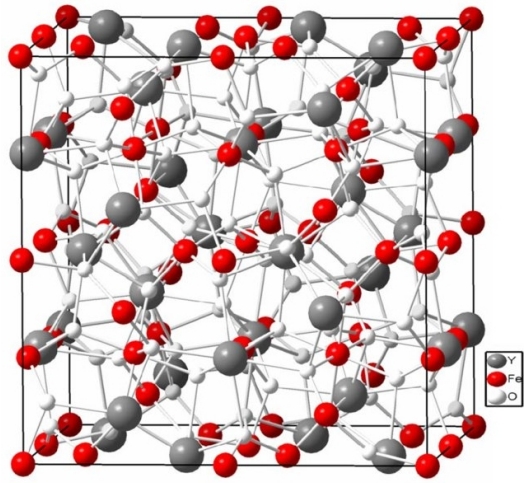

Figure 3. The complex unit cell of the yttrium iron garnet (YIG) phase.

For the forging experiments, the ferritic alloy powder was blended with the reactive YIG powder in the proportion of 99.40-0.60 wt.%, respectively. Eight cube-shaped cans were fabricated by powder bed selected laser deposition using 316L stainless steel (SS) powder. The length of the sides of the cube was 4 cm. A 1 mm thick sheet of 316L SS was purchased for the top of the can, and a 0.25 in. diameter hole was drilled in the center of the top, to which a 0.25 in. diameter SS tube was welded for the purpose of degassing the powder. Each can was filled with ~400 g of blended powder, and the top with the degassing tube was welded to the cube-shaped can. Figure 4 shows the unfilled cube-shaped cans and the fully assembled can with the degassing tube. The filled cans were degassed under vacuum for 6 h at 300°C, and the tube was crimped and cut.

Two forging presses exist at ORNL for compacting the powder filled cans at elevated temperatures: a 350-ton press and a 50-ton press. The 350-ton press has controls for the displacement rate of the press, whereas the 50-ton press has one displacement rate. The procedure for performing a forging experiment is shown in Figure 5. The can is placed in one of three open air furnaces set at a particular temperature and held for a designated time (Fig. 5a). The furnace door is opened, the can is placed on the mount block in the forging press, and then the press is activated. The cube shown in Figure 5b was heated for 2 h at 1,000°C and pressed on three sides to 30% deformation.

After the forging experiments were completed, four ~1 cm cubed-shaped samples were cut and mounted with the three orthogonal surface directions facing up. These three faces were labeled F, for face, containing the degassing tube and T1 and T2 for the two normal directions to F. The surfaces were polished to a final finish of 0.06 mm colloidal silica and were examined by optical microscopy. The fourth sample was ground on each side to ensure removal of the HIP 316L SS can and was used for density measurements by the Archimedes method.

(a) (b)

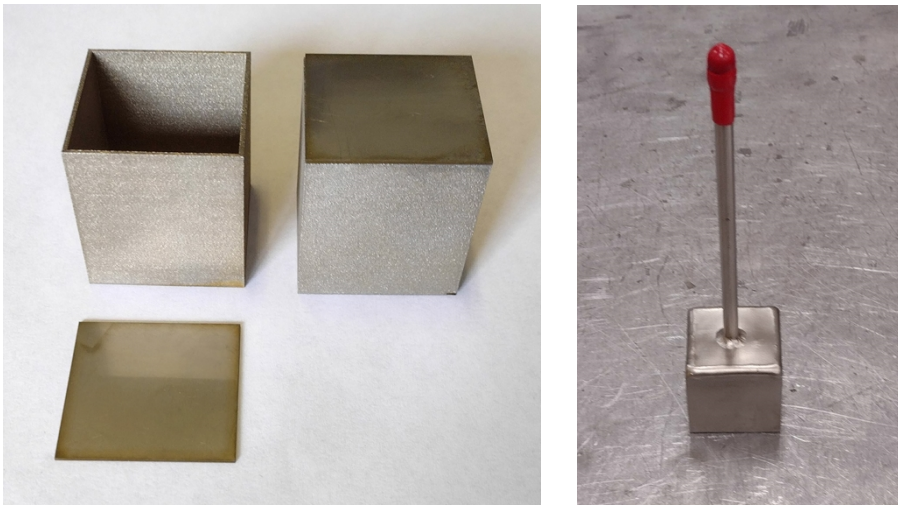

Figure 4. Construction of the cube-shaped can for filling with the reactive YIG and ferritic alloy powders. (a) the bottom section of two cube-shaped cans fabricated by powder bed selective laser melting using 316L SS powder and the thin sheet of 316L SS and (b) the final construction of the cube-shaped can with the top 316L SS sheet and 0.25 in. SS tube welded together.

(a) (b)

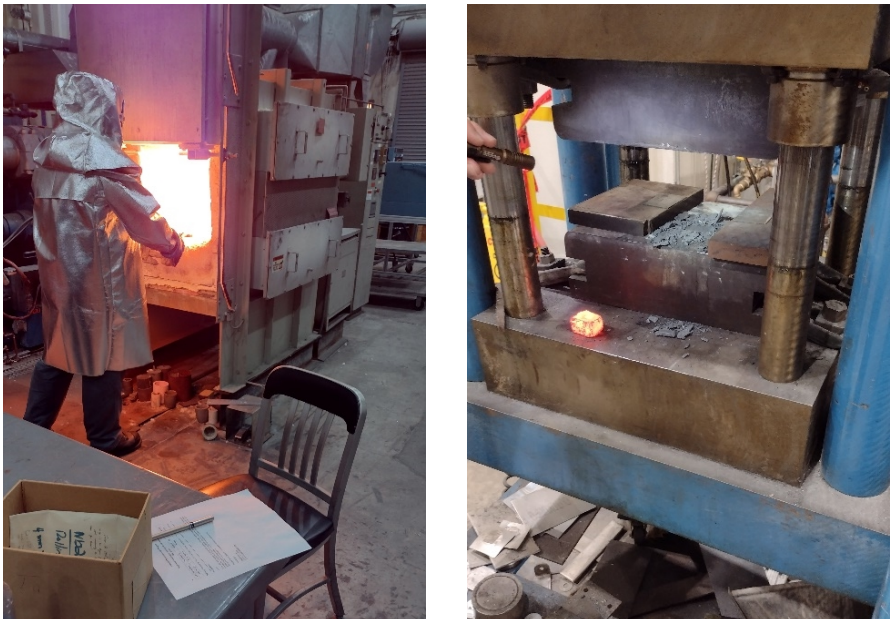

Figure 5. The procedure for performing a forging experiment. (a) removing the powder filled can from the furnace after 2 h at 1,000°C and (b) the can after forging to 30% on the three sides.

4. RESULTS AND DISCUSSION

A set of forging conditions was initially chosen to achieve this work package's goal of producing an ODS ferritic alloy. The first step was to place the filled can in an open-air furnace set at 1,000°C for 2 h. The objective of this heat treatment was to sinter the powders to initiate the densification process. After removing the can from the furnace, it was forged to 30% deformation on each of the three sides using the 50-ton press. This first forging run is referred to as *Hi*, for high-temperature heat treatment. The can was then placed in a different furnace set at 500°C and held for 1 h, followed by forging to 30% deformation on each of the three sides. The goal of this combination of heat treatment and forging was to increase the dislocation density and form sub-grain structures in the microstructure of the ferritic alloy powders. This second heat treatment and forging run is referred to as *Lo*, for low-temperature heat treatment. The final forging condition is to place the can in a third furnace set at 800°C for 1 h, followed by forging to 30% on each of the three sides, which is referred to as *Me*. The objective of this combination of heat treatment and forging was to consolidate the powders to full or near-full density and to trigger dynamic recrystallization processes. It is during dynamic recrystallization that the grain boundaries will migrate in the microstructure, causing grains to continually form and disappear; this is the mechanism that will facilitate the dissolution of the reactive YIG particles and redistribution of the constituent Y, Fe, and O elements through the microstructure of the BCC ferritic alloy. This third heat treatment and forging condition is referred to as *Me*, for medium-temperature heat treatment.

The first forging experiment was conducted on the HiLoMe-1 sample, which consisted of all three heat treatments and forging parameters listed above. Figure 6 shows optical micrographs of the microstructures observed in the HiLoMe-1 and Hi-1 with the F orientation. The surface conditions are unetched to reveal the porosity caused by incomplete densification of the powder. The remnants of the sintered powders indicate that there is no prominent anisotropy in the particle shape. This is a result of the forging compaction on the each of the three sides of the cube-shaped can. The results indicate that there is less porosity in the HiLoMe-1 sample compared to the Hi-1 sample, which is consistent with the three heat treatment and forging parameters for the former sample compared to the single initial sintering heat treatment and forging for the latter sample.

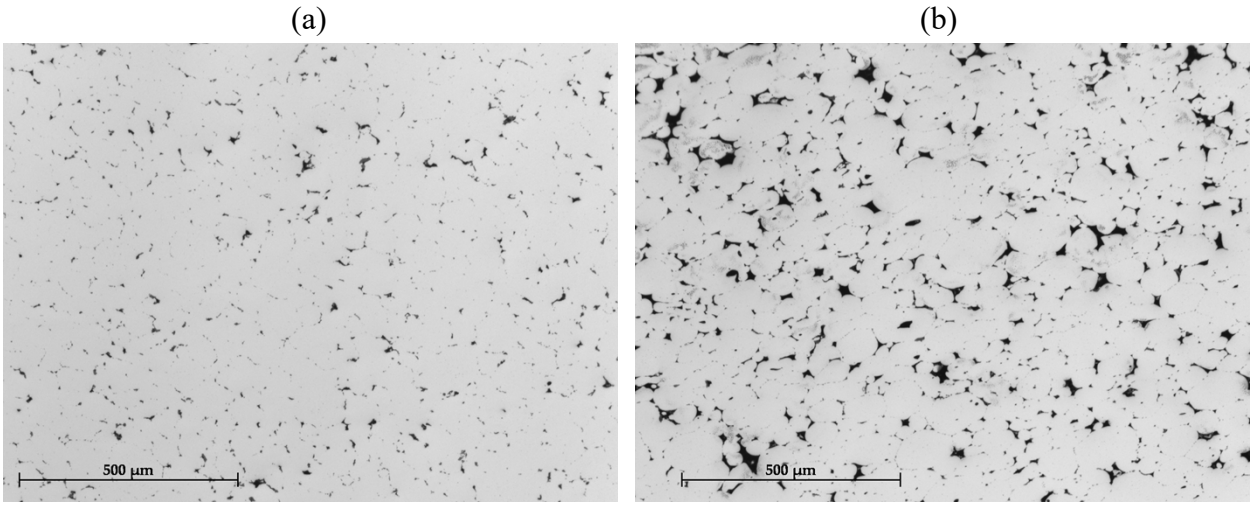

Figure 6. Optical micrographs showing the front orientations for (a) the HiLoMe-1 sample and (b) the Hi-1 sample.

For assessment of the porosity, the particle analysis tool in ImageJ was applied to the optical micrographs of HiLoMe-1 and Hi-1 samples in the T1 orientation. The procedures involved applying a fast Fourier

transform (FFT) bandpass filter set at typically 20% to the region of interest (ROI) image. This image was then adjusted using the threshold option to obtain the best correlation of black and white for the pores distributed in the microstructure. The porosity was then analyzed by creating an outline of each pore and then measuring the area of each pore. The area associated with each numbered pore is stored in an Excel spreadsheet for analysis. The volume fraction of the porosity is calculated by dividing the total area of the pores by the area of the ROI image. Figures 7 and 8 show the ROI and outline images of the porosity observed in the microstructures of the HiLoMe-1 sample and the Hi-1 sample, respectively. The results indicated that the volume fraction of porosity in the HiLo-Me-1 sample was ~2.49% and ~5.70% for the Hi-1 sample. Although the densification in both samples is incomplete, these results provide insights into the effects of changing heat treatments and forging parameters to improve the densification of the powders after the initial sintering heat treatment and forging compaction.

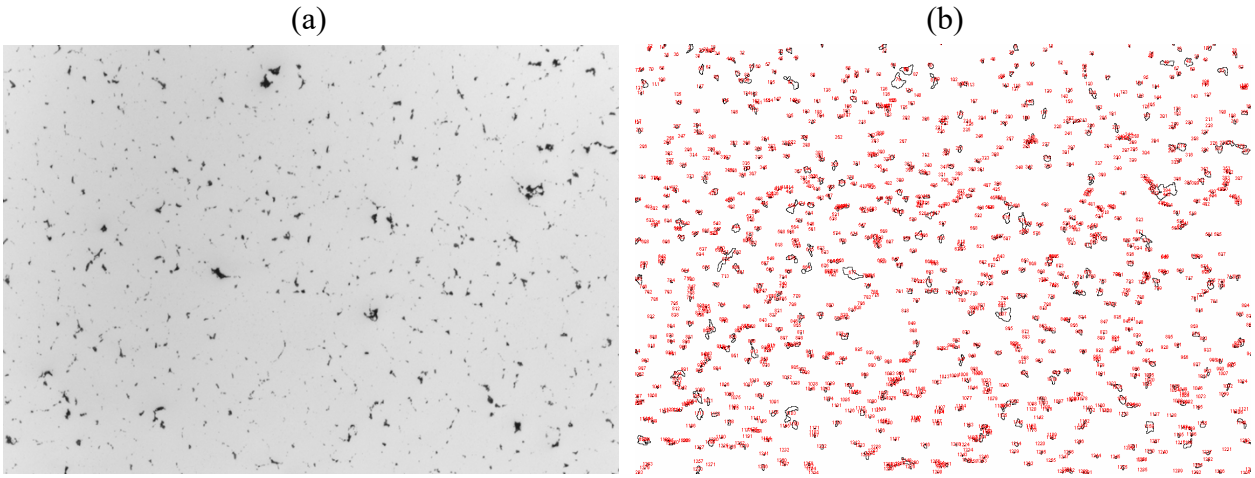

Figure 7. Porosity analysis of the HiLoMe-1 sample in the L1 orientation. (a) Reduced area of interest (RAI) for the threshold setting and (b) the outline of features in the RAI for porosity analysis.

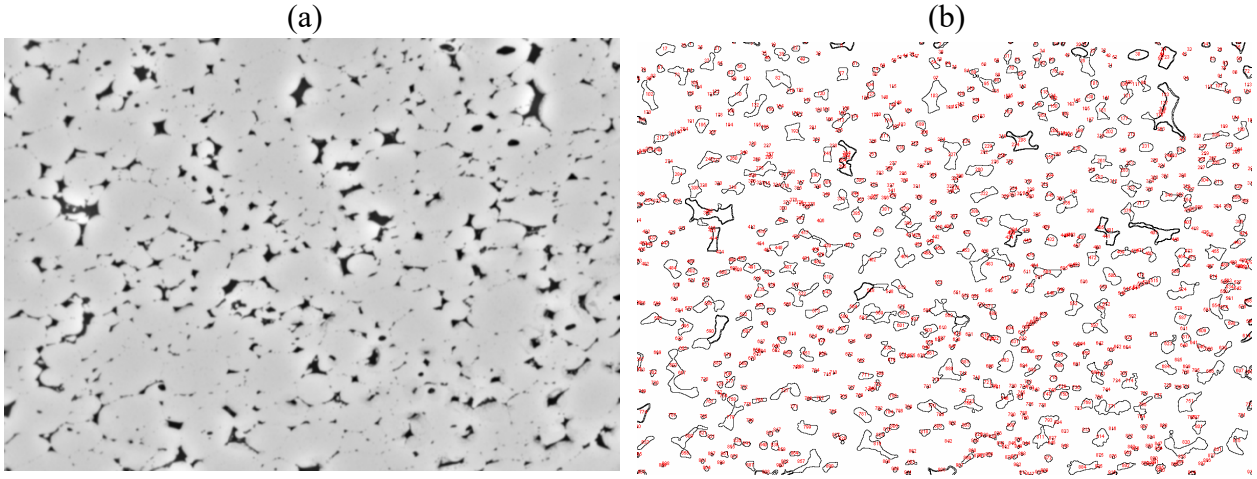

Figure 8. Porosity analysis of the Hi-1 sample in the L1 orientation. (a) Reduced area of interest (RAI) for the threshold setting and (b) the outline of features in the RAI for porosity analysis.

5. CONCLUSIONS

This report summarizes recent efforts under the Innovative Nuclear Materials program to produce an ODS ferritic alloy for advanced reactor fuel cladding applications. In the final quarter of FY23, work centered on (1) selecting the reactive powder, $Y_3Fe_5O_{12}$ yttrium iron garnet (YIG), and the ferritic alloy powder, Fe-10Cr-1W-0.3Ti-0.2V (wt %); (2) preparing 316L SS cans for filling with blended powder followed by degassing; and (3) choosing the heat treatments and forging parameters for performing the first two forging experiments. Optical microscopy on polished yet unetched surfaces of samples cut in three orthogonal directions revealed remnant porosity in both samples. The analysis of the porosity revealed a lower amount of ~2.49% in the HiLoMe-1 sample that was processed with the three heat treatments and forging parameters compared to ~5.70% for the Hi-1 sample that was processed with only the first sintering heat treatment and forging parameter. Although the densification in both samples is incomplete, these initial results will provide insights toward the goal of improving the densification of the powders, especially after the initial sintering heat treatment and forging compaction. In FY24, the optimum heat treatments and forging parameters for achieving the dispersion of nano-size oxide particles in the microstructure of the ODS Fe-10Cr ferritic alloy will be investigated, supported by detailed microstructure characterization studies. A new larger batch of Ar gas atomized powder will be procured to produce a large ODS ferritic alloy ingot with optimized composition and forging parameters for mechanical properties testing.

6. REFERENCES

[1] S. Ukai, M. Harada, H. Okada, M. Inoue, S. Nomura, S. Shikakura, K. Asabe, T. Nishida, M. Fujiwara, Alloying design of oxide dispersion for long life FBRs core materials. *Journal of Nuclear Materials*. **204** (1993) 65-73.

[2] R. Lindau, A. Möslang, M. Schirra, P. Schlossmacher, M. Klimenkov. Mechanical and microstructural properties of a hipped RAFM ODS-steel. *Journal of Nuclear Materials*. 307-311 (2002) 769-772.

[3] S. Ukai, M. Fujiwara, Perspective of ODS alloys application in nuclear environments. *Journal of Nuclear Materials*. 307-311 (2002) 749-757.

[4] I.-S. Kim, C.-Y Kang, B.-Y Choi, T. Okuda, P.J. Maziasz, K. Miyahara, Effect of Ti and W on the Mechanical Properties and Microstructure of 12% Cr Base Mechanical-alloyed Nano-sized ODS Ferritic Alloys *ISIJ International*. **43** (10) (2003) 1640-1646.

[5] S. Ukai, S. Ohtsuka, Nano-mesoscopic structure control in 9Cr–ODS ferritic steels. *Energy Materials* **2** (1) (2007) 26-35.

[6] D.T. Hoelzer, J. Bentley, M.A. Sokolov, M.K. Miller, G.R. Odette, M.J. Alinger, Influence of particle dispersions on the high-temperature strength of ferritic alloys. *Journal of Nuclear Materials*. 367-370 (2007) 166-172.

[7] Y. de Carlan, J.-L. Bechade, P. Dubuisson, J.-L. Seran, P. Billot, A. Bougault, T. Cozzika, S. Doriot, D. Hamon, J. Henry, M. Ratti, N. Lochet, D. Nunes, P. Olier, T. Leblond, M.H. Mathon, CEA developments of new ferritic ODS alloys for nuclear applications. *Journal of Nuclear Materials*. 386–388 (2009) 430-432.

[8] M.J. Alinger, G.R. Odette, D.T. Hoelzer, On the role of alloy composition and processing parameters in nanocluster formation and dispersion strengthening in nanostructured ferritic alloys. *Acta Mater*. **57** (2009) 392-406.

[9] N. Baluc, J.L. Boutard, S.L. Dudarev, M. Rieth, J. Brito Correia, B. Fournier, J. Henry, F. Legendre, T. Leguey, M. Lewandowska, R. Lindau, E. Marquis, A. Muñoz, B. Radiguet, Z. Oksiuta, Review on the EFDA work programme on nanostructured ODS RAF steels. *Journal of Nuclear Materials*. **417** (2011) 149-153.

[10] A. Kimura, R. Kasada, N. Iwata, H. Kishimoto, C.H. Zhang, J. Isselin, P. Dou, J.H. Lee, N. Muthukumar, T. Okuda, M. Inoue, S. Ukai, S. Ohnuki, T. Fujiwara, T.F. Abe, Development of Al added high-Cr ODS steels for fuel cladding of next generation nuclear systems. *Journal of Nuclear Materials*. **417** (2011) 176-179.

[11] H. Hadraba, B. Kazimierzak, L. Stratil, I. Dlouhy, Microstructure and impact properties of ferritic ODS ODM401 (14%Cr-ODS of MA957 type). *Journal of Nuclear Materials*. **417** (2011), 241-244.

[12] M.S. Nagorka, C.G. Levi, G.E. Lucas and S.D. Ridder, The potential of rapid solidification in oxide-dispersion-strengthened copper alloy development. *Materials Science and Engineering A*, **142** (1991), 277-289.

[13] A.M. Redsten, E.M. Klier, A.M Brown, D.C. Dunand, Mechanical properties and microstructure of cast oxide-dispersion-strengthened aluminum. *Materials Science and Engineering A,* **201**, (1995), 88-102.

[14] M.A. Moghadas, M. Nili-Ahmadabadi, F. Forchani, H.S. Kim, Development of an oxide dispersion-strengthened steel by introducing oxygen carrier compound into the melt aided by a general thermodynamic model. *Scientific Reports*, **6**, (2016), 38621.

[15] H. Jia, Z. Zhou, S. Li, A new strategy for additive manufacturing ODS steel using Y-containing gas atomized powder. *Materials Characterization*, 187, (2015), 111876.

[16] T. Boegelein, S.N. Dryepondt, A. Pandey, K. Dawson, G.J. Tatlock, Mechanical response and deformation mechanisms of ferritic oxide dispersion strengthened steel structures produced by selective laser melting. *Acta Materialia*, **87**, (2015), 201-205.

[17] B.M. Arkurst, J.H. Bae, M.Y. Na, H.J. Chang, H.G. Kim, I.H. Kim, H.J. Ryu, J.H. Kim, Effect of tellurium on the microstructure and mechanical properties of Fe-14Cr oxide-dispersion-strengthened steels produced by additive manufacturing. *Journal of Materials Science & Technology*, **95**, (2021), 114-126.

[18] R. Gao, L. Zeng, H. Ding, T. Zhang, X. Wang, Q. Fang, Characterization of oxide dispersion strengthened ferritic steel fabricated by electron beam selective melting. *Materials and Design*, 89, (2016), 1171-1180.

[19] J. Bentley, D.T. Hoelzer, L. Chaffron, D.W. Coffey, K.A. Yarborough, Element Mapping of Reaction Ball Milled Y-Ni-O Nanostructure. *Microscopy and Microanalysis*, **10** (Suppl. 2) (2004), 494-495.

[20] N. Sallez, Recrystallization, abnormal grain growth and ultrafine microstructure of ODS ferritic steels. *Materials*. Université de Grenoble, 2014. English. <NNT : 2014GRENI075.